

Article pubs.acs.org/JPCC

# Singlet-to-Triplet Spin Transitions Facilitate Selective 1-Butene Formation during Ethylene Dimerization in Ni(II)-MFU-4/

Jenna L. Mancuso, Carlo A. Gaggioli, Laura Gagliardi,\* and Christopher H. Hendon\*



Cite This: J. Phys. Chem. C 2021, 125, 22036-22043



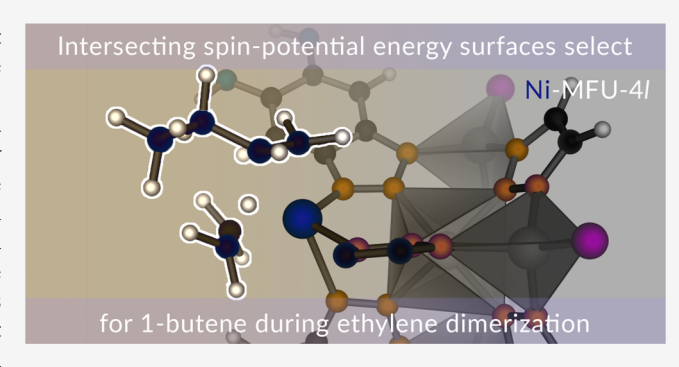
**ACCESS** I

Metrics & More



Supporting Information

ABSTRACT: Catalytic ethylene dimerization is an important chemical reaction that suffers from a lack of selectivity for the desired product, 1-butene. Metal-organic frameworks (MOFs) bearing Ni-based catalytic sites have been shown to yield record selectivity for 1-butene. Early efforts to understand this selectivity revealed that chain propagation and 2-butene formation are competitive with 1-butene, seemingly at odds with experimental evidence that these products are disfavored. Here, we present an alternative mechanism for selective 1-butene formation in the highest performing MOF, Ni(II)-MFU-4l. Our study reveals competing electronic spin configuration pathways that intersect along the reaction coordinate. Intersystem crossing provides an



explanation for the selective formation of 1-butene in the MOF. Furthermore, we explore intersystem crossing as a unique design principle for MOF catalyst design and highlight a departure from conventional molecular catalyst design paradigms.

#### ■ INTRODUCTION

Fossil fuel dependence creates an uncertain future for energy production and commodities derived from crude oil. In particular, 1-butene—a linear  $\alpha$ -olefin produced and consumed on the megaton scale each year<sup>2</sup>—is used in diesel production and as a precursor to other value-added products. 3,4 Traditionally, 1-butene is a product of oligomerization or fragmentation processes that typically yield a distribution of C<sub>n</sub>-backbone products (i.e., alkenes and alkanes of various carbon lengths).5,6 While most 1-butene comes from petroleum cracking processes, it can also be formed selectively through ethylene dimerization.<sup>7,8</sup> However, ethylene dimerization catalysts suffer from competitive formation of 2-butene and longer chain alkenes, pointing to a need to develop more selective ethylene dimerization catalysts.

Current industrial ethylene dimerization technologies employ homogeneous Ni(II) and Co(II) metal complexes, which have some shortcomings compared to heterogeneous catalysts (e.g., heterogeneous architectures, in principle, allow for continuous processing with longer catalyst lifetimes and recyclability). 12 Surface-anchored equivalents tend to be poorly characterized or feature an array of reactivity based on differences in the local chemical environment. 13 An ideal ethylene dimerization catalyst would embody the advantages of both technologies, allowing for molecular design of catalytic sites in heterogeneous scaffolds.<sup>14</sup>

Conveniently, metal-organic frameworks (MOFs) are an emergent class of porous, 15 crystalline catalysts 16-18 that demonstrate efficacy for the conversion of ethylene to 1butene. 19-21 The ability to create site-isolated active sites, 22

through either pre- or postsynthetic approaches, 23,24 has enabled the precise design of molecular-like catalytic sites built into the MOF. MOFs featuring isolated Ni(II) sites with precisely tuned inner-sphere ligation have offered a promising heterogeneous alternative to current industrial catalysts.<sup>25-</sup> These nickel-based MOFs can be directly synthesized<sup>28</sup> or obtained through postsynthetic grafting,<sup>29</sup> deposition,<sup>30,31</sup> and metathesis.<sup>32</sup> However, state-of-the-art MOF catalysts are still known to produce the undesired product 2-butene, as well as a marginal amount of 1-hexene.

In previous work, 1-butene selectivity achieved within Ni(II)-MOF catalysts has been attributed to higher activation barriers for chain propagation than termination (and subsequent release of 1-butene).<sup>33</sup> Selectivity toward the  $\alpha$ olefin product has been rationalized by comparing the activation barriers for isomerization with  $\beta$ -hydride elimination (BHE).<sup>34</sup> However, the magnitude of these differences in the activation barrier is relatively small (e.g., 0.5 kcal/mol difference between chain termination and propagation for Ni(II)-NU-1000<sup>33</sup>) or thermally accessible (e.g., 3.5 kcal/mol difference in primary and secondary Ni-alkyl binding along the

Received: August 30, 2021 Revised: September 7, 2021 Published: October 1, 2021





isomerization route for Ni(II)-MFU-4l, computed along a consistent Ni(II) singlet pathway).<sup>34</sup>

In a recent experimental report, the Ni(II)-containing MOF Ni(II)-MFU-4*l* achieved 1-butene selectivity surpassing the current industrial technologies.<sup>35</sup> Ethylene dimerization is thought to occur at the Kuratowski-type secondary building unit (SBU, see Figure 1).<sup>35</sup> While the conventional Kuratowski

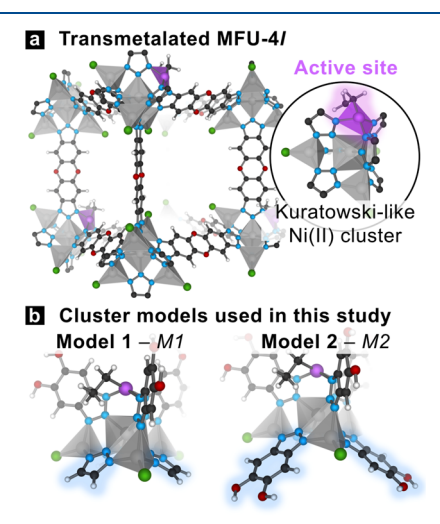


**Figure 1.** (a) MFU-4l features Kuratowski clusters that, upon metal exchange, host distorted square-planar  $S_0$ –Ni(II). (b) Computationally, these clusters can be truncated from the parent MOF by peripheral triazines (model 1, M1) or with inclusion of the aromatic diol (model 2, M2). Both models are used in this study, but all reaction coordination diagrams depict energies from M1.

cluster is a pentanuclear Zn(II),  $^{36,37}$  at least one peripheral Zn(II) may be exchanged for Ni(II), accessing a scorpionate reagent cavity similar to the molecular scaffold, nickel tris(pyrazolyl)borate, that affords high 1-butene selectivity.  $^{38}$  Ni(II)-MFU-4l exhibits >96% selectivity for the  $C_4$  product 1-butene, exceeding the 81% selectivity achieved with the homogeneous analogue.  $^{35}$  Ethylene dimerization in this material is known to proceed via the typical Cossee-Arlmantype mechanism (Figure 2) as determined through isotopic labeling experiments in conjunction with density functional theory calculations.  $^{34}$  However, the driving force for the exceptional selectivity of this catalyst for the linear  $\alpha$ -olefin product over the internal olefin, 2-butene, remains largely unknown.

Here, we employ quantum mechanical simulations to elucidate the underlying electronic forces that drive 1-butene formation and prevent isomerization and propagation. We present a mechanistic investigation along both accessible spin surfaces (where the Ni center may alternate between a ground state singlet and triplet) and compare the zero-point energycorrected free-energy profiles of ethylene dimerization and competing pathways over Ni(II) in both MFU-4l and the homogeneous trispyrazolyl borate analogue. We show that intersystem crossing (ISC) at critical transition states (which we refer to as spin-switching) contributes to selectivity for 1butene.<sup>39</sup> This spin-switching mechanism highlights an overlooked aspect of MOF catalysis—the ability to access nonground-state potential energy surfaces during chemical transformations—and promotes the requirement to look beyond the crystallographic structure of MOFs to understand their reactivity. 40

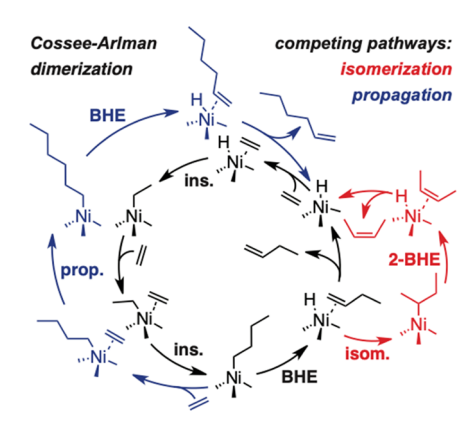


Figure 2. Ni(II) catalysts have been shown to dimerize ethylene through the Cossee–Arlman mechanism—the same mechanism through which higher-order olefins are produced (propagation pathway shown in blue). The isomerization pathway to form 2-butene is shown in red. Selectivity for a single insertion to the  $C_4$  product is contingent on BHE occurring prior to, and faster than, isomerization (i.e., H-insertion to the  $\alpha$ -carbon and subsequent BHE).

**Computational Methods.** The unit cell for MFU-4l contains two pentanuclear Zn(II) nodes (Figure S5). By exchanging a single Zn(II) per unit cell with Ni(II), Ni(10%)-MFU-4l is formed. Bulk Ni(10%)-MFU-4l was fully optimized using the PBEsol functional<sup>41</sup> as implemented in the Vienna ab initio Software Package (VASP)<sup>42–44</sup> using 500 eV cutoff for the projector-augmented-wave plane-wave basis. Ionic and electronic energy convergence criteria of 0.005 eV and 1 ×  $10^{-6}$  eV, respectively, were applied to a 2 × 2 × 2  $\Gamma$ -centered k-grid. All solid-state optimizations proceeded with the same methods.

Two cluster models were extracted from the optimized periodic structure, and any bonds severed in the extraction process were passivated with the addition of hydrogen atoms (H<sup>•</sup>). In model 1 (M1, Figure 1b), the bistriazolatedibenzodioxin (BTDD) linkers around the active site were bisected, inclusive of the dioxin oxygen atoms, while linkers on the opposite side of the cluster were truncated to the triazolate motif. To ensure that this approximation did not result in asymmetric electronics that impact the reaction cycle, we compared the Cossee-Arlman dimerization pathway M1 with a second model in which all linkers were truncated at the dioxin motif (M2, Figure 1b) on both the singlet and triplet energy surfaces. Based on previous experimental and computational assessments of the ethylene dimerization mechanism for Ni(II)-MFU-4l, we know that the reaction proceeds through a Cossee-Arlman-type mechanism rather than a metallocycle.<sup>3</sup> We additionally considered  $\beta$ -hydrogen transfer as an alternate chain termination event but found the activation energy for this pathway to be >30 kcal/mol larger than for the expected BHE pathway and therefore likely inactive (Table S1).

Consistent with prior investigations of ethylene dimerization in Ni(II)-containing MOFs<sup>33</sup> and similar systems, <sup>45</sup> computations were performed on molecular cluster models using the M06-L<sup>46</sup> functional as implemented in Gaussian09. <sup>47</sup> Metal atoms (Zn/Ni) were treated with a doubly polarized triple- $\zeta$  basis set (def2-tzvpp), while all other atoms were treated with a polarized split-valence basis set (def2-svp). <sup>48</sup> The same methods were employed to compute triplet and singlet energy

pathways for the homogeneous analogues<sup>38</sup> shown in Figure 5b. All structures are presented in Supporting Information.

The coordinates of terminal oxygen or carbon atoms were kept fixed in M2 and M1, respectively, to mimic lattice stabilization from MOF incorporation in extracted cluster models. Vibrational analysis was performed at 298.15 K to obtain thermodynamic quantities, including the zero-point energy correction, and confirm potential energy surface minima and saddle points with zero and one imaginary frequency, respectively. The gas-phase  $\Delta G$  is computed at 298.15 K to account for the zero-point energy. The computation of the minimum energy crossing point (MECP) was performed using a program described by Harvey et al. 49 interfaced with the Gaussian package and the computational details described above.

## ■ RESULTS AND DISCUSSION

Native tetrahedral Zn(II)—Cl sites found in MFU-4l are catalytically inert, yet the postsynthetic modification of these sites via transmetalation with Ni(II), and subsequent treatment with an initiator such as methylaluminoxane, yields a catalytically active species, Figure 1b.<sup>35</sup> Although four-coordinate Ni(II) centers typically adopt a square-planar coordination geometry with a singlet ground state, within the Kuratowski cluster, Ni(II) obtains a four-coordinate tetrahedral geometry and a ground state triplet, Figure 3. However,

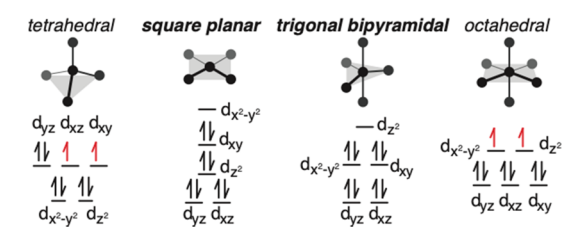


**Figure 3.** Spin state of a transition metal-containing system will be dependent on both the ligand field strength, which determines the dorbital spitting energy, and the coordination number and geometry. Throughout the course of a catalytic cycle, each of these parameters is dynamic.

tantamount to ethylene dimerization is the requirement for the metal to dynamically bind ethylene to an open-metal site.<sup>50</sup> It should not be surprising, then, that throughout the course of a catalytic cycle, a change in inner-sphere ligation—based on the

coordination number and configuration—may also affect the active spin surface, potentially inducing ISC (per idealized coordination geometries, as presented in Figure 3).<sup>45,51–53</sup>

In an idealized nonpolarized coordination environment, both tetrahedral and octahedral Ni(II) complexes are expected to be ground-state triplets, while both square-planar and five-coordinate species are expected to be singlets. <sup>54</sup> This variability presents an inherent modeling challenge: how should one treat a transition state that likely undergoes a spin reconfiguration upon the dynamic binding or insertion of a reagent? In these cases of atypical coordination geometry and changes in the coordination number, it is important to consider both spin surfaces and their potential crossings.

To assess the dimerization, isomerization, and propagation pathways in Ni(II)-MFU-4l, we first isolated two cluster models to evaluate the impact of peripheral ligands on the Kuratowski cluster, Figure 1b. Both models keep the SBU containing the entire Zn<sub>4</sub>Ni inorganic unit and six connecting triazolate motifs intact. Since steric effects at the catalytic active site are a long-known contributor to selectivity for short-chain olefins over longer chains or polymers, 55 the BTDD linkers around the active site were bisected, inclusive of the dioxin oxygen atoms in both models. In model 1 (M1, Figure 1b), the linkers on the allosteric side of the cluster were truncated to the pyrazolate motif to reduce computational expense. In model 2 (M2, Figure 1b), all linkers were truncated at the dioxin motifs to assess the role of cluster symmetry and any electronic dipole artifacts. All bonds severed by extraction were passivated by hydrogen atoms to saturate the valence orbitals.<sup>22</sup>

Following the Cossee-Arlman dimerization mechanism, we compared the energetics of M1 and M2 along the main reaction pathway. With both models, we found that alkylbound species (four-coordinate) favor a triplet spin state and that no equilibrium geometry could be identified for olefin-bound species in the triplet state (i.e., the ethylene does not bind to the metal). However, the inclusion of extended allosteric ligands in M2 resulted in a smaller difference between the singlet and triplet spin surfaces at stationary points throughout the reaction by 2.3–4.0 kcal/mol. Regardless, the same reaction profile was recovered using both models, including predicted ISC events and relative activation barriers between reaction steps, Figure S2. For the remainder of this paper, however, we selected M1 to balance the computational

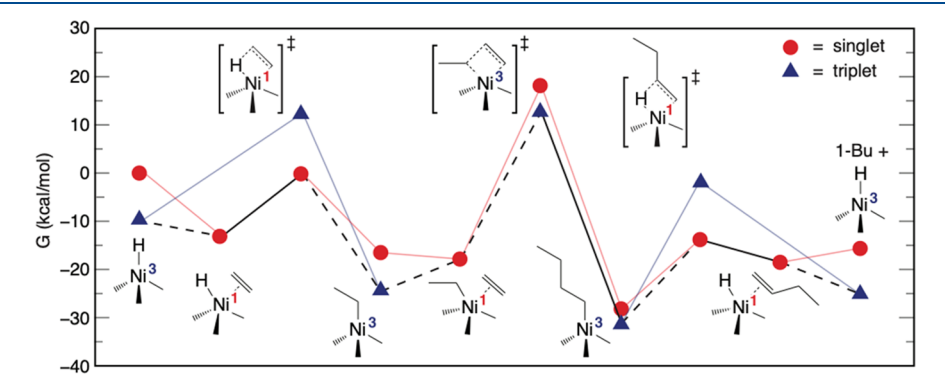
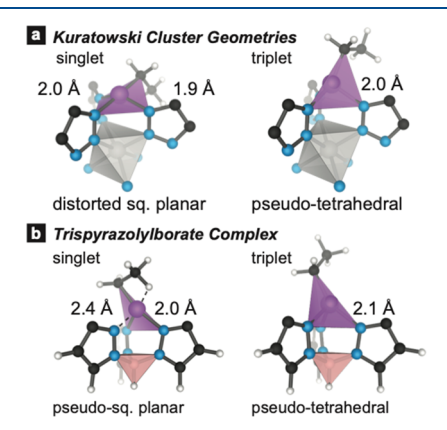


Figure 4. Singlet (red circles, red lines) and triplet (blue triangles, blue lines) dimerization energy surfaces experience repeated crossing when plotted with the singlet Ni—H species and two free ethylene molecules as the absolute reference, indicating that the lowest energy reaction route (black lines) incorporates both spin surfaces, that is, the Ni(II) spin state is dynamic throughout the catalytic cycle. Atom economy is maintained throughout the cycle by including one or zero equivalents of free ethylene in the free energy of each intermediate along the reaction coordinate.

cost and electronic structure accuracy while exploring both spin surfaces along each competitive reaction pathway, as detailed in Figure 2.

By plotting the reaction profile of a single catalyst turnover to yield 1-butene on the triplet-state energy surface (Figure 4, blue) relative to the singlet energy surface (Figure 4, red), it is apparent that the spin surfaces repeatedly intersect throughout the lowest energy mechanistic pathway (Figure 4, dotted black lines). Hydride insertion and elimination events are expected to take place on the singlet spin surface; the transition state energies for ethylene to ethyl conversion and butyl to 1-butene conversion recovered from singlet configurations are 12.6 and 12.3 kcal/mol lower in energy, respectively, than the triplet configurations. However, the resulting alkyl-substituted active sites exhibit lower energy triplet geometries. At key stationary points throughout the dimerization pathway, we see that the triplet and singlet energy differences diminish as the chain length, that is, the electron-donating ability of the metal-bound alkyl, increases: the triplet geometry is 9.2, 7.4, and 2.8 kcal/ mol more stable than the singlet geometry for Ni<sup>II</sup>(H), Ni<sup>II</sup>(Et), and Ni<sup>II</sup>(Bu), respectively. We expect the triplet Ni<sup>II</sup>(H) system to play a significant role as an energetic sink to accelerate 1-butene expulsion from the singlet configuration (last step in Figure 4).56 Experimental investigation of the same catalyst for propylene dimerization found reinsertion of 1-butene to be slow and product distribution to be dependent on the primary olefin insertion event.<sup>57</sup> This is consistent with the recovered spin-switching mechanism where 1-butene desorption is favored only through relaxation to the stable ground-state triplet of the tetrahedral nickel hydride. While 1butene desorption is uphill in energy by 2.8 kcal/mol on the singlet spin surface, spin-switching affords exergonic product release that is downhill in energy by 6.4 kcal/mol.

Taking a closer look at the coordination sphere of Ni(II) in each spin state, we find that the active-site geometry for the singlet Ni<sup>II</sup>(R) MOF species is distorted square planar, Figure 5a. A similar geometric trend is observed for the analogous homogeneous catalyst Tp<sup>Mes</sup>NiCl,<sup>38</sup> but we note that Ni(II) is more labile in the molecular complex; the singlet geometry



**Figure 5.** Ni(II)-alkyl species adopt a distorted square-planar geometry in the singlet state and a seesaw geometry in the triplet state in both homogeneous and MOF-incorporated active sites. The selected bond lengths depicted for these systems show reduced Ni–N bond lengths in the Kuratowski cluster (a) relative to the molecular catalyst (b), but the Ni–N bond for both triplet geometries is equivalent. The symmetry of the triplet geometry is likely reinforced in the crystal lattice, evident from the large singlet—triplet gap computed with periodic boundary conditions.

features a partial dissociation of the N-donor ligand (Figure 5b) and  $\beta$ -hydrogen bonding with the unbound nitrogen. In contrast, a nearly tetrahedral geometry is adopted by both systems in the triplet state. Within the MOF, the alkyl chain tail bisects two neighboring BTDD ligands in both the singlet and triplet configurations, likely to mitigate steric interactions between the growing chain and the linkers. Prior to olefin coordination, the nontriazolate ligand (H, Et, Bu, and Hex) is nearly axial in the triplet state. However, the olefin approach, especially under high pressures, can further distort the triplet toward the more open distorted square-planar ligand arrangement that allows for the side-on association of the small ethylene molecule in the singlet state. This coordinationinduced spin-switching phenomenon has been observed in other Ni(II) complexes with rigid N-donor ligands. 52,53,58,59 We note that the axial position of the growing alkyl chain and orientation of linker protons that point directly at the active site likely shield the metal from coordinating larger olefins and inhibit subsequent transformations of preferentially desorbed 1-butene products to longer olefins or isomers.

To examine the feasibility of ISC, we explored the spin-surface intersection along the reaction coordinate for olefin insertion to yield Ni<sup>II</sup>(Bu). While spin—orbit coupling may be used to assess these transitions, its inclusion is often impermissible due to the system size. Here, the system contains first-row transition metals and organics, so spin—orbit coupling effects are likely to be small. Therefore, the MECP will lie close in energy to the transition state in the adiabatic surface and is a good approximation to the transition state computed with spin—orbit coupling. By analyzing each spin surface between Ni<sup>II</sup>(Et)( $\eta^2$ -Et) and Ni<sup>II</sup>(Bu) as discussed in Supporting Information, we find that the MECP occurs after C–C formation. At this point, Ni(II) can spin-switch from singlet to triplet, enabling a pathway to form the triplet Ni<sup>II</sup>(Bu) intermediate.

Olefin coordination to Ni<sup>II</sup>(Bu)( $\eta^2$ -Et) is 10.3 kcal/mol lower in energy and seemingly functions as a potential well. To perform BHE on the singlet PES, the system would have to expel the bound ethylene to pass through the MECP to the triplet Ni<sup>II</sup>(Bu). However, butyl chain orientation following the insertion step must enable the olefin approach for ethylene adsorption to occur in the first place. Conveniently, the identified MECP geometry for ethylene insertion is similar to the activated complex for BHE (Figure S4); a  $\beta$ -agostic interaction facilitates BHE by reducing the necessary reconfiguration. The MECP is lower in energy than the BHE transition state energy on the singlet PES by 6.8 kcal/mol (Figure S4), so spin-switching does not impact the ratedetermining barrier for BHE in the singlet transition state. Previous work on a zeolite-based Ni(II)-ethylene dimerization catalyst showed that there is a free-energy penalty associated with displacing the hydrocarbon chain for ethylene association.<sup>61</sup> In other words, ethene coordination was found to be disfavored in the presence of a butyl chain due to the requisite rotation to afford the coordinative approach. Resultantly, C-C coupling proceeded on mobile active sites that detached upon ethylene coordination to adopt the preferred square-planar Ni(II) complex. This release of bonding constraints is unattainable for metals incorporated directly into the clusterbased nodes of Ni(II)-MFU-4l, which grants access to the spin-switching mechanism deduced here. By hindering ethylene coordination once a single insertion has occurred, propagation is restricted and butene selectivity is enhanced.

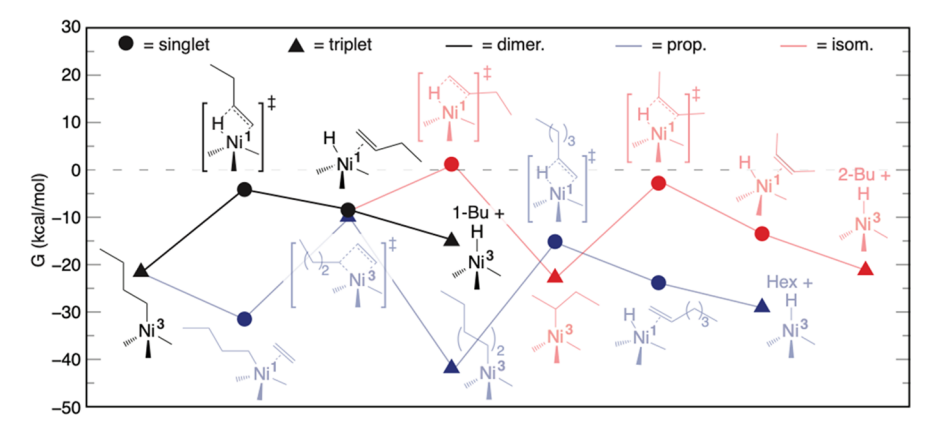


Figure 6. Lowest energy reaction pathways for ethylene dimerization, propagation, and isomerization via the Cossee–Arlmann mechanism are overlaid to reveal that following the first ethylene insertion to form a  $C_4$ -paraffin, isomerization to 2-butene is endergonic by ~0.6 kcal/mol, while 1-butene formation and propagation remain exergonic relative to the nickel hydride species. The barrier for BHE (black), however, is 17.3 kcal/mol, while α-hydride insertion (red), 2°-BHE (red), and propagation (blue) have activation barriers of 9.6 kcal/mol, 19.9 kcal/mol, and 22.3 kcal/mol, respectively. The activation barrier to propagation is >5 kcal/mol larger in magnitude than the barrier that leads directly to 1-butene release. For isomerization, while the activation barrier to isomerization from the preceding intermediate is lower than that of BHE, the activated complex is 5.2 kcal/mol higher in Gibbs free energy than that of BHE. Furthermore, this transformation is in direct competition with 1-butene release, which is exergonic by 6.4 kcal/mol.

To assess the implication of ISC on the overall 1-butene selectivity, we additionally explored the net energetic pathways for isomerization to the C<sub>4</sub>-product 2-butene and propagation to the C<sub>6</sub>-product 1-hexene by identifying the lowest energy spin configuration for each intermediate and activated complex at each step of the reaction, Figure 6. Evidently, double-bond migration is effectively suppressed despite the thermodynamic stability of the internal olefin (Figure 6, red). In order to form 2-butene, following BHE, an  $\alpha$ -hydride insertion must occur rather than 1-butene desorption. This hydride shift forms a 2°alkyl species that is responsible for the subsequent hydride elimination step to 2-butene. While the 2°-alkyl intermediate is 1.6 kcal/mol more stable than the 1°-alkyl intermediate, the Gibbs free energy of the  $\alpha$ -hydride insertion transition state necessary for its formation is 5.2 kcal/mol greater than the preceding BHE and 0.6 kcal/mol greater than the Ni<sup>II</sup>(H) starting point, whereas BHE is 4.7 kcal/mol lower in Gibbs free energy from the same starting point. Importantly,  $\alpha$ hydride insertion is in direct competition with the barrierless release of 1-butene, favored relative to isomerization by 16.0 kcal/mol. Combined with the 5.2 kcal/mol higher transition state energy for  $\alpha$ -hydride insertion relative to BHE, 1-butene formation and release are more likely to occur than isomerization to 2-butene.

While the pathway for isomerization is endergonic relative to the nickel hydride species on the triplet surface, both BHE and propagation barriers are entirely downhill from the nickel hydride species (and two or three equivalents of free ethylene in the case of C<sub>4</sub> and C<sub>6</sub> products, respectively) by 4.7 and 9.9 kcal/mol. At first glance, the propagation pathway seems to be favorable. Indeed, the conversion of C–C  $\pi$ -bonds to C–C  $\sigma$ bonds is the thermodynamic driving force for common polymerization catalysts. 62,63 However, the activation barrier for propagation is 5.0 kcal/mol greater than the barrier for 1°-BHE, driving the equilibrium toward chain termination events. Unlike isomerization, which is only possible following BHE, propagation is in direct competition with 1-butene formation. As previously discussed, ethylene coordination blocks BHE. However, the dissociation of ethylene from Ni<sup>II</sup>(Bu)( $\eta^2$ -Et) only has an energetic penalty of 10.3 kcal/mol compared with

the 22.3 kcal/mol activation barrier for propagation to occur. Given that butyl chains are known to kinetically hinder the olefin approach to the active site<sup>61</sup> and that intersystem crossing facilitates BHE, 1-butene desorption is more likely to occur than hexene formation.

To understand the implications of MOF incorporation on both selectivity and spin state, we finally compared the reaction profile of our cluster model with the homogeneous catalyst that inspired its design on both spin surfaces, Figure S3. In homogeneous systems, where only the local active site is defined, bulky ligands are shown to favor linear chain formation rather than hinder propagation, while more open active sites afford greater rates of BHE and, therefore, a Schulz-Flory distribution of oligomers rather than polymers. 64,65 Contrary to the predetermined Kuratowski cluster geometry where BTDD linkers connect six metals from two different nodes, the Tp<sup>Mes</sup> chelating ligand of the single metal homogeneous analogue can dissociate an N-donor to accommodate changes to the coordination environment without necessitating a change in the spin state. The active site can be opened for BHE to occur on the singlet surface, while the mesityl functionalities provide the steric blockage necessary to prevent isomerization.

The entropic freedom of catalysts in the solution phase affords equilibrium structures for olefin-bound intermediates on both spin surfaces. The singlet geometry for Tp<sup>Mes</sup>Ni<sup>II</sup>(Et) exploits its entropic freedom to grant a  $\beta$ -agostic interaction with the bound alkyl functionality (Figure 5b). However, the pseudotetrahedral triplet geometry remains lower in energy by 15.6 kcal/mol for Ni<sup>II</sup>(H) and 5.6 kcal/mol for both Ni<sup>II</sup>(Et) and Ni<sup>II</sup>(Bu) (Figure S3). Still, olefin coordination results in significantly higher energy structures for the triplet configuration (e.g., 19.5 and 20.3 kcal/mol for Ni<sup>II</sup>(H)( $\eta^2$ -Et) and  $Ni^{II}(Et)(\eta^2-Et)$ , respectively). It is, therefore, possible that the same spin-switching phenomenon afforded by MFU-4l is active in the Tp<sup>Mes</sup> analogue. However, unlike in the MOF-catalyst, the only species more stable as triplets than singlets are the four-coordinate alkyl intermediates. Rather than olefin dissociation, followed by association, direct olefin substitution may occur such that no ISC occurs in the solution phase.<sup>66</sup>

The more labile coordination geometry means that unlike in the MOF-based catalyst, the ligand sphere of the molecular complex can distort to accommodate olefin association leading to propagation and the wider transition state geometries associated with isomerization, lowering 1-butene selectivity.

Thermally accessible spin-switching events are known for other Ni(II) trispyrazolyl borate systems.<sup>67</sup> Four-coordinate molecular Ni(II) diimine chain transfer polymerization catalysts also exhibited natural spin switching between lowspin square-planar geometries and high-spin tetrahedral geometries throughout the catalytic cycle.<sup>68</sup> Structural changes in the ligands, such as altering the location and direction of steric bulk, granted synthetic spin-state control by the resultant coordination geometry distortions, consistent with our results. Closer to the explored catalyst structure, four-coordinate Ni(II)-Me complexes with strongly donating tris-carbene borate ligands exhibit the same seesaw geometry observed here in the triplet state, as well as the distorted square-planar geometry of the singlet (Figure 5).<sup>69</sup> Although the carbene system resulted in a more stable singlet state than the triplet, tuning electron density around the metal atom to distort the ligand field could easily alter the preference.

In homogeneous complexes, the flexible Ni(II) coordination sphere can be both distorted and rigidified by multidentate ancillary ligands with strong electron-donating abilities to facilitate ISC and BHE. <sup>45,51,70,71</sup> Here, the mutual accessibility of spin surfaces known for Ni<sup>II</sup> systems with rigid N-donor ligands is accessed through postsynthetic cluster incorporation from heterogenization in a MOF. Thus, with knowledge of how ligand spheres affect the coordination geometry and the subsequent material spin state, it is possible to tune the singlet—triplet energy gap and control ISC events. By comparing transition state geometries with spin-state geometries, we can target reaction pathways by targeting the corresponding spin state. Beyond nitrogenic ligand spheres, molecular complexes including both nitrogenic and phosphoric donors yield exceptional electrocatalytic hydrogen uptake kinetics and may be attractive future targets. <sup>72,73</sup>

## CONCLUSIONS

In sum, we have found that the inclusion of Ni(II) into the scorpionate-type MFU-4l nodes undergoes ISC and electronically disfavors both isomerization and propagation. The transition state free energy for  $\alpha$ -hydride insertion toward isomerization is 5.2 kcal/mol higher than that of BHE, and the activation barrier for propagation is 5.0 kcal/mol greater than that of BHE. The resultant 1-butene selectivity is afforded, in part, by a geometrically restricted active site that is both open enough to favor BHE and sufficiently narrow to disfavor both nonlinear chain growth and olefin approach with C<sub>4</sub> hydrocarbons. This work also highlights the critical role of intersecting spin surfaces in transition metal-mediated catalytic pathways. We propose that the contribution of transient triplet state species accessed through effectively barrierless ISC events further favors product expulsion due to the condensed nature of Ni<sup>II</sup>(H) and the sizeable triplet-singlet energy gap associated with this specific species (9.2 kcal/mol compared with 2.8 kcal/mol for Ni<sup>II</sup>(Bu)). Our results also point to a general observation that increased selectivity can be achieved by operating at lower temperatures, where ISC and the resultant competing product pathways are thermally disfavored.

Altogether, we predict that the conical active site of the MOF hinders olefin approach with C<sub>4</sub> species present and that ISC drives both BHE and 1-butene expulsion. The concept of utilizing ISC to enhance product selectivity is novel. It offers a wealth of new theoretical and experimental avenues while also highlighting the utility of unique coordination spheres afforded by MOFs, especially those that have been transmetalated. Other materials capable of merely grafting catalytic components cannot provide the same inherent bulk stabilization of the distorted ligand sphere that we find facilitates BHE. The accessibility of unique coordination geometries from lattice stabilization is an encouraging property for MOF catalyst design because the mutual dependence of the geometry and electronic configuration enables fine-tuning of the overall transition metal reactivity.

#### ASSOCIATED CONTENT

# **5** Supporting Information

The Supporting Information is available free of charge at https://pubs.acs.org/doi/10.1021/acs.jpcc.1c07658.

Supplementary figures, including comparison of cluster models, reaction trajectories for these models, and example simulated nickel hydride IR spectra (PDF) Supplementary tables, including comparisons with hybrid GGA functionals and summaries of reaction barriers, and equilibrium geometry structure files for reaction intermediates and transition states (ZIP)

# AUTHOR INFORMATION

#### **Corresponding Authors**

Laura Gagliardi — Department of Chemistry, Pritzker School of Molecular Engineering, James Franck Institute, University of Chicago, Chicago, Illinois 60637, United States; orcid.org/0000-0001-5227-1396; Email: lgagliardi@uchicago.edu

Christopher H. Hendon – Department of Chemistry and Biochemistry, University of Oregon, Eugene, Oregon 97403, United States; orcid.org/0000-0002-7132-768X; Email: chendon@uoregon.edu

#### **Authors**

Jenna L. Mancuso – Department of Chemistry and Biochemistry, University of Oregon, Eugene, Oregon 97403, United States

Carlo A. Gaggioli — Department of Chemistry, Pritzker School of Molecular Engineering, James Franck Institute, University of Chicago, Chicago, Illinois 60637, United States

Complete contact information is available at: https://pubs.acs.org/10.1021/acs.jpcc.1c07658

#### **Author Contributions**

The manuscript was written through contributions of all authors. All authors have given approval to the final version of the manuscript.

#### Notes

The authors declare no competing financial interest.

## ACKNOWLEDGMENTS

The authors acknowledge the Minnesota Supercomputing Institute (MSI) at the University of Minnesota for providing computational resources. The computational work at Oregon was enabled by the NSF-supported XSEDE program [grant

ACI-1548562] and is supported in part by the National Science Foundation through the Division of Materials Research under Grant DMR-1956403. C.A.G. and L.G. were supported as part of the Inorganometallic Catalysis Design Center, an Energy Frontier Research Center funded by the U.S. Department of Energy, Office of Science, Basic Energy Sciences, under Award DE-SC0012702.

#### REFERENCES

- (1) Shafiee, S.; Topal, E. When Will Fossil Fuel Reserves Be Diminished? *Energy Policy* **2009**, 37, 181–189.
- (2) Bender, M. An Overview of Industrial Processes for the Production of Olefins C<sub>4</sub> Hydrocarbons. *ChemBioEng Rev.* **2014**, *1*, 136–147
- (3) Liu, L.; Harris, T. D. Metal—Organic Frameworks as Potential Catalysts for Industrial 1-Butene Production. ACS Cent. Sci. 2016, 2, 125—127.
- (4) Muraza, O. Maximizing Diesel Production through Oligomerization: A Landmark Opportunity for Zeolite Research. *Ind. Eng. Chem. Res.* **2015**, *54*, 781–789.
- (5) Britovsek, G. J. P.; Malinowski, R.; McGuinness, D. S.; Nobbs, J. D.; Tomov, A. K.; Wadsley, A. W.; Young, C. T. Ethylene Oligomerization beyond Schulz-Flory Distributions. *ACS Catal.* **2015**, *5*, 6922–6925.
- (6) Gollwitzer, A.; Dietel, T.; Kretschmer, W. P.; Kempe, R. A Broadly Tunable Synthesis of Linear  $\alpha$ -Olefins. *Nat. Commun.* **2017**, 8, 1226.
- (7) Mohsenzadeh, A.; Zamani, A.; Taherzadeh, M. J. Bioethylene Production from Ethanol: A Review and Techno-Economical Evaluation. *ChemBioEng Rev.* **2017**, *4*, 75–91.
- (8) Hulea, V. Toward Platform Chemicals from Bio-Based Ethylene: Heterogeneous Catalysts and Processes. *ACS Catal.* **2018**, *8*, 3263–3279.
- (9) Fischer, K.; Jonas, K.; Misbach, P.; Stabba, R.; Wilke, G. n. The? Nickel Effect? *Angew. Chem., Int. Ed.* 1973, 12, 943–953.
- (10) Ziegler, K. Aluminium-organische Synthese im Bereich olefinischer Kohlenwasserstoffe. *Angew. Chem.* **1952**, *64*, 323–329.
- (11) Ziegler, K.; Holzkamp, E.; Breil, H.; Martin, H. Das Mülheimer Normaldruck-Polyäthylen-Verfahren. *Angew. Chem.* **1955**, *67*, 541–547.
- (12) Kaiser, S. K.; Chen, Z.; Faust Akl, D.; Mitchell, S.; Pérez-Ramírez, J. Single-Atom Catalysts across the Periodic Table. *Chem. Rev.* **2020**, *120*, 11703–11809.
- (13) Bordiga, S.; Groppo, E.; Agostini, G.; van Bokhoven, J. A.; Lamberti, C. Reactivity of Surface Species in Heterogeneous Catalysts Probed by In Situ X-Ray Absorption Techniques. *Chem. Rev.* **2013**, *113*, 1736–1850.
- (14) Qin, R.; Liu, K.; Wu, Q.; Zheng, N. Surface Coordination Chemistry of Atomically Dispersed Metal Catalysts. *Chem. Rev.* **2020**, 120, 11810–11899.
- (15) Farha, O. K.; Eryazici, I.; Jeong, N. C.; Hauser, B. G.; Wilmer, C. E.; Sarjeant, A. A.; Snurr, R. Q.; Nguyen, S. T.; Yazaydın, A. Ö.; Hupp, J. T. Metal—Organic Framework Materials with Ultrahigh Surface Areas: Is the Sky the Limit? *J. Am. Chem. Soc.* **2012**, *134*, 15016—15021.
- (16) Stubbs, A. W.; Braglia, L.; Borfecchia, E.; Meyer, R. J.; Román-Leshkov, Y.; Lamberti, C.; Dincă, M. Selective Catalytic Olefin Epoxidation with Mn<sup>II</sup>-Exchanged MOF-5. *ACS Catal.* **2018**, *8*, 596–601.
- (17) Seo, J. S.; Whang, D.; Lee, H.; Jun, S. I.; Oh, J.; Jeon, Y. J.; Kim, K. A Homochiral Metal—Organic Porous Material for Enantioselective Separation and Catalysis. *Nature* **2000**, *404*, 982—986.
- (18) Manna, K.; Ji, P.; Lin, Z.; Greene, F. X.; Urban, A.; Thacker, N. C.; Lin, W. Chemoselective Single-Site Earth-Abundant Metal Catalysts at Metal—Organic Framework Nodes. *Nat. Commun.* **2016**, *7*, 12610.

- (19) Yang, D.; Gates, B. C. Catalysis by Metal Organic Frameworks: Perspective and Suggestions for Future Research. *ACS Catal.* **2019**, *9*, 1779–1798.
- (20) Konnerth, H.; Matsagar, B. M.; Chen, S. S.; Prechtl, M. H. G.; Shieh, F.-K.; Wu, K. C.-W. Metal-Organic Framework (MOF)-Derived Catalysts for Fine Chemical Production. *Coord. Chem. Rev.* **2020**, *416*, 213319.
- (21) Pascanu, V.; González Miera, G.; Inge, A. K.; Martín-Matute, B. Metal-Organic Frameworks as Catalysts for Organic Synthesis: A Critical Perspective. *J. Am. Chem. Soc.* **2019**, *141*, 7223–7234.
- (22) Mancuso, J. L.; Mroz, A. M.; Le, K. N.; Hendon, C. H. Electronic Structure Modeling of Metal—Organic Frameworks. *Chem. Rev.* **2020**, *120*, 8641–8715.
- (23) Kalaj, M.; Cohen, S. M. Postsynthetic Modification: An Enabling Technology for the Advancement of Metal–Organic Frameworks. ACS Cent. Sci. 2020, 6, 1046–1057.
- (24) Yaghi, O. M.; O'Keeffe, M.; Ockwig, N. W.; Chae, H. K.; Eddaoudi, M.; Kim, J. Reticular Synthesis and the Design of New Materials. *Nature* **2003**, *423*, 705–714.
- (25) Forestière, A.; Olivier-Bourbigou, H.; Saussine, L. Oligomerization of Monoolefins by Homogeneous Catalysts. *Oil Gas Sci. Technol.* **2009**, *64*, 649–667.
- (26) Al-Sherehy, F. A. Studies in Surface Science and Catalysis; Elsevier, 1996; Vol. 100, pp 515–523.IFP-SABIC Process for the Selective Ethylene Dimerization to Butene-1 DOI: 10.1016/s0167-2991(96)80052-8
- (27) Suttil, J. A.; McGuinness, D. S. Mechanism of Ethylene Dimerization Catalyzed by  $Ti(OR')_4/AlR_3$ . Organometallics **2012**, 31, 7004–7010.
- (28) Griffin, S. L.; Champness, N. R. A Periodic Table of Metal-Organic Frameworks. *Coord. Chem. Rev.* **2020**, *414*, 213295.
- (29) Madrahimov, S. T.; Gallagher, J. R.; Zhang, G.; Meinhart, Z.; Garibay, S. J.; Delferro, M.; Miller, J. T.; Farha, O. K.; Hupp, J. T.; Nguyen, S. T. Gas-Phase Dimerization of Ethylene under Mild Conditions Catalyzed by MOF Materials Containing (Bpy)Ni <sup>II</sup> Complexes. ACS Catal. 2015, 5, 6713–6718.
- (30) Li, Z.; Schweitzer, N. M.; League, A. B.; Bernales, V.; Peters, A. W.; Getsoian, A. B.; Wang, T. C.; Miller, J. T.; Vjunov, A.; Fulton, J. L.; Lercher, J. A.; Cramer, C. J.; Gagliardi, L.; Hupp, J. T.; Farha, O. K.; Farha, O. K. Sintering-Resistant Single-Site Nickel Catalyst Supported by Metal—Organic Framework. J. Am. Chem. Soc. 2016, 138, 1977—1982.
- (31) Klet, R. C.; Wang, T. C.; Fernandez, L. E.; Truhlar, D. G.; Hupp, J. T.; Farha, O. K. Synthetic Access to Atomically Dispersed Metals in Metal—Organic Frameworks via a Combined Atomic-Layer-Deposition-in-MOF and Metal-Exchange Approach. *Chem. Mater.* **2016**, 28, 1213—1219.
- (32) Evans, J. D.; Sumby, C. J.; Doonan, C. J. Post-Synthetic Metalation of Metal-Organic Frameworks. *Chem. Soc. Rev.* **2014**, *43*, 5933–5951.
- (33) Bernales, V.; League, A. B.; Li, Z.; Schweitzer, N. M.; Peters, A. W.; Carlson, R. K.; Hupp, J. T.; Cramer, C. J.; Farha, O. K.; Gagliardi, L. Computationally Guided Discovery of a Catalytic Cobalt-Decorated Metal—Organic Framework for Ethylene Dimerization. *J. Phys. Chem. C* 2016, 120, 23576—23583.
- (34) Metzger, E. D.; Comito, R. J.; Hendon, C. H.; Dincă, M. Mechanism of Single-Site Molecule-Like Catalytic Ethylene Dimerization in Ni-MFU-4 l. *J. Am. Chem. Soc.* **2017**, *139*, 757–762.
- (35) Metzger, E. D.; Brozek, C. K.; Comito, R. J.; Dincă, M. Selective Dimerization of Ethylene to 1-Butene with a Porous Catalyst. *ACS Cent. Sci.* **2016**, *2*, 148–153.
- (36) Bunzen, H.; Grzywa, M.; Kalytta-Mewes, A.; Volkmer, D. One-Pot Synthesis of Ultrastable Pentanuclear Alkylzinc Complexes. *Dalton Trans.* **2017**, *46*, 2618–2625.
- (37) Liu, Y.-Y.; Grzywa, M.; Tonigold, M.; Sastre, G.; Schüttrigkeit, T.; Leeson, N. S.; Volkmer, D. Photophysical Properties of Kuratowski-Type Coordination Compounds  $[M^{II}Zn_4Cl_4(Me_2bta)_6]$  ( $M^{II}=Zn$  or Ru) Featuring Long-Lived Excited Electronic States. Dalton Trans. 2011, 40, 5926–5938.

- (38) Kunrath, F. A.; de Souza, R. F.; Casagrande, O. L.; Brooks, N. R.; Young, V. G. Highly Selective Nickel Ethylene Oligomerization Catalysts Based on Sterically Hindered Tris(Pyrazolyl)Borate Ligands. Organometallics 2003, 22, 4739–4743.
- (39) Biswas, S.; Tonigold, M.; Speldrich, M.; Kögerler, P.; Weil, M.; Volkmer, D. Syntheses and Magnetostructural Investigations on Kuratowski-Type Homo- and Heteropentanuclear Coordination Compounds  $[MZn_4Cl_4(L)_6]$  ( $M^{II} = Zn$ , Fe, Co, Ni, or Cu; L = 5,6-Dimethyl-1,2,3-Benzotriazolate) Represented by the Nonplanar  $K_{3,3}$  Graph. *Inorg. Chem.* **2010**, *49*, 7424–7434.
- (40) Allendorf, M. D.; Stavila, V.; Witman, M.; Brozek, C. K.; Hendon, C. H. What Lies beneath a Metal—Organic Framework Crystal Structure? New Design Principles from Unexpected Behaviors. J. Am. Chem. Soc. 2021, 143, 6705—6723.
- (41) Perdew, J. P.; Burke, K.; Ernzerhof, M. Generalized Gradient Approximation Made Simple. *Phys. Rev. Lett.* **1996**, *77*, 3865–3868.
- (42) Kresse, G.; Furthmüller, J. Efficiency of Ab-Initio Total Energy Calculations for Metals and Semiconductors Using a Plane-Wave Basis Set. *Comp. Mater. Sci.* **1996**, *6*, 15–50.
- (43) Kresse, G.; Furthmüller, J. Efficient Iterative Schemes for Ab Initio Total-Energy Calculations Using a Plane-Wave Basis Set. *Phys. Rev. B: Condens. Matter Mater. Phys.* **1996**, *54*, 11169–11186.
- (44) Kresse, G.; Hafner, J. Ab Initio Molecular-Dynamics Simulation of the Liquid-Metal–Amorphous-Semiconductor Transition in Germanium. *Phys. Rev. B: Condens. Matter Mater. Phys.* **1994**, 49, 14251–14269.
- (45) Farcaş, A.-A.; Bende, A. Improving the Light-Induced Spin Transition Efficiency in Ni(II)-Based Macrocyclic-Ligand Complexes. *Molecules* **2019**, *24*, 4249.
- (46) Zhao, Y.; Truhlar, D. G. A New Local Density Functional for Main-Group Thermochemistry, Transition Metal Bonding, Thermochemical Kinetics, and Noncovalent Interactions. *J. Chem. Phys.* **2006**, 125, 194101.
- (47) Frisch, M. J.; Trucks, G. W.; Schlegel, H. B.; Scuseria, G. E.; Robb, M. A.; Cheeseman, J. R.; Scalmani, G.; Barone, V.; Petersson, G. A.; Nakatsuji, H.; et al. *Gaussian 09*. Revision A.02; Gaussian, Inc.: Wallingford CT, 2009.
- (48) Weigend, F.; Ahlrichs, R. Balanced Basis Sets of Split Valence, Triple Zeta Valence and Quadruple Zeta Valence Quality for H to Rn: Design and Assessment of Accuracy. *Phys. Chem. Chem. Phys.* **2005**, *7*, 3297–3305.
- (49) Harvey, J. N.; Aschi, M.; Schwarz, H.; Koch, W. The Singlet and Triplet States of Phenyl Cation. A Hybrid Approach for Locating Minimum Energy Crossing Points between Non-Interacting Potential Energy Surfaces. *Theor. Chem. Acc.* **1998**, *99*, 95–99.
- (50) Arrozi, U. S. F.; Bon, V.; Kutzscher, C.; Senkovska, I.; Kaskel, S. Towards Highly Active and Stable Nickel-Based Metal—Organic Frameworks as Ethylene Oligomerization Catalysts. *Dalton Trans.* **2019**, *48*, 3415–3421.
- (51) Brandenburg, H.; Krahmer, J.; Fischer, K.; Schwager, B.; Flöser, B.; Näther, C.; Tuczek, F. Coordination-Induced Spin-State Switching with Nickel(II) Salpn Complexes: Electronic versus Steric Effects and Influence of Intermolecular Interactions: Coordination-Induced Spin-State Switching with Nickel(II) Salpn Complexes: Electronic versus Steric Effects and Influence of Intermolecular Interactio. *Eur. J. Inorg. Chem.* 2018, 2018, 576–585.
- (52) Dommaschk, M.; Schütt, C.; Venkataramani, S.; Jana, U.; Näther, C.; Sönnichsen, F. D.; Herges, R. Rational Design of a Room Temperature Molecular Spin Switch. The Light-Driven Coordination Induced Spin State Switch (LD-CISSS) Approach. *Dalton Trans.* **2014**, *43*, 17395–17405.
- (53) Homma, Y.; Ishida, T. A New S=0, ⇒S=2 "Spin-Crossover" Scenario Found in a Nickel(II) Bis(Nitroxide) System. *Chem. Mater.* **2018**, *30*, 1835–1838.
- (54) Gray, H. B.; Ballhausen, C. J. A Molecular Orbital Theory for Square Planar Metal Complexes. *J. Am. Chem. Soc.* **1963**, 85, 260–265.
- (55) Wilke, G.; Bogdanović, B.; Hardt, P.; Heimbach, P.; Keim, W.; Kröner, M.; Oberkirch, W.; Tanaka, K.; Steinrücke, E.; Walter, D.;

- Zimmermann, H. Allyl-Transition Metal Systems. *Angew. Chem., Int. Ed.* **1966**, *5*, 151–164.
- (56) Breitenfeld, J.; Vechorkin, O.; Corminboeuf, C.; Scopelliti, R.; Hu, X. Why Are  $(NN_2)Ni$  Pincer Complexes Active for Alkyl–Alkyl Coupling:  $\beta$ -H Elimination Is Kinetically Accessible but Thermodynamically Uphill. *Organometallics* **2010**, *29*, 3686–3689.
- (57) Comito, R. J.; Metzger, E. D.; Wu, Z.; Zhang, G.; Hendon, C. H.; Miller, J. T.; Dincă, M. Selective Dimerization of Propylene with Ni-MFU-4 l. *Organometallics* **2017**, *36*, 1681–1683.
- (58) Venkataramani, S.; Jana, U.; Dommaschk, M.; Sonnichsen, F. D.; Tuczek, F.; Herges, R. Magnetic Bistability of Molecules in Homogeneous Solution at Room Temperature. *Science* **2011**, *331*, 445–448.
- (59) Thies, S.; Bornholdt, C.; Köhler, F.; Sönnichsen, F. D.; Näther, C.; Tuczek, F.; Herges, R. Coordination-Induced Spin Crossover (CISCO) through Axial Bonding of Substituted Pyridines to Nickel-Porphyrins:  $\sigma$ -Donor versus  $\pi$ -Acceptor Effects. *Chem.—Eur. J.* **2010**, *16*, 10074–10083.
- (60) Gaggioli, C. A.; Belpassi, L.; Tarantelli, F.; Harvey, J. N.; Belanzoni, P. Spin-Forbidden Reactions: Adiabatic Transition States Using Spin-Orbit Coupled Density Functional Theory. *Chem.—Eur. J.* **2018**, *24*, 5006–5015.
- (61) Brogaard, R. Y.; Kømurcu, M.; Dyballa, M. M.; Botan, A.; Van Speybroeck, V.; Olsbye, U.; De Wispelaere, K. Ethene Dimerization on Zeolite-Hosted Ni Ions: Reversible Mobilization of the Active Site. *ACS Catal.* **2019**, *9*, 5645–5650.
- (62) Cossee, P. Mechanism of Polymerization of a-Olefins with Ziegler-Natta Catalysts. *J. Catal.* **1964**, *3*, 80–88.
- (63) Grubbs, R.; Tumas, W. Polymer Synthesis and Organotransition Metal Chemistry. *Science* **1989**, 243, 907–915.
- (64) Killian, C. M.; Johnson, L. K.; Brookhart, M. Preparation of Linear  $\alpha$ -Olefins Using Cationic Nickel(II)  $\alpha$ -Diimine Catalysts. Organometallics 1997, 16, 2005–2007.
- (65) Chen, C. Designing Catalysts for Olefin Polymerization and Copolymerization: Beyond Electronic and Steric Tuning. *Nat. Rev. Chem.* **2018**, *2*, 6–14.
- (66) Agirrezabal-Telleria, I.; Luz, I.; Ortuño, M. A.; Oregui-Bengoechea, M.; Gandarias, I.; López, N.; Lail, M. A.; Soukri, M. Gas Reactions under Intrapore Condensation Regime within Tailored Metal—Organic Framework Catalysts. *Nat. Commun.* **2019**, *10*, 2076.
- (67) Ma, H.; Petersen, J. L.; Young, V. G.; Yee, G. T.; Jensen, M. P. Solid-State Spin Crossover of Ni(II) in a Bioinspired N<sub>3</sub>S<sub>2</sub> Ligand Field. *J. Am. Chem. Soc.* **2011**, 133, 5644–5647.
- (68) Vitek, A. K.; Leone, A. K.; McNeil, A. J.; Zimmerman, P. M. Spin-Switching Transmetalation at Ni Diimine Catalysts. *ACS Catal.* **2018**, *8*, 3655–3666.
- (69) Hill, E. A.; Zhao, N.; Filatov, A. S.; Anderson, J. S. Nickel(II)-Methyl Complexes Adopting Unusual Seesaw Geometries. *Chem. Commun.* **2020**, *56*, 7861–7864.
- (70) Wang, J.; Alam, F.; Chang, Q.; Chen, Y.; Jiang, T. Catalytic Behavior Tuning via Structural Modifications of Silylated-diphosphine Ni(II) Complexes for Ethylene Selective Dimerization. *Appl. Organomet. Chem.* **2020**, 34, No. e5722.
- (71) Froese, R. D. J.; Musaev, D. G.; Morokuma, K. Theoretical Study of Substituent Effects in the Diimine–M(II) Catalyzed Ethylene Polymerization Reaction Using the IMOMM Method. *J. Am. Chem. Soc.* **1998**, *120*, 1581–1587.
- (72) Helm, M. L.; Stewart, M. P.; Bullock, R. M.; DuBois, M. R.; DuBois, D. L. A Synthetic Nickel Electrocatalyst with a Turnover Frequency Above 100,000 s<sup>-1</sup> for H<sub>2</sub> Production. *Science* **2011**, 333, 863–866.
- (73) Hou, J.; Fang, M.; Cardenas, A. J. P.; Shaw, W. J.; Helm, M. L.; Bullock, R. M.; Roberts, J. A. S.; O'Hagan, M. Electrocatalytic H  $_2$  Production with a Turnover Frequency  $>10^7$  s  $^{-1}$ : The Medium Provides an Increase in Rate but Not Overpotential. *Energy Environ. Sci.* **2014**, *7*, 4013–4017.